Article

Photoinduced Axial Ligation and Deligation Dynamics of Nonplanar Nickel Dodecaarylporphyrins

Jennifer L. Retsek, Charles Michael Drain, Christine Kirmaier, Daniel J. Nurco, Craig J. Medforth, Kevin M. Smith, Igor V. Sazanovich, Vladimir S. Chirvony, Jack Fajer, and Dewey Holten

J. Am. Chem. Soc., **2003**, 125 (32), 9787-9800• DOI: 10.1021/ja020611m • Publication Date (Web): 19 July 2003

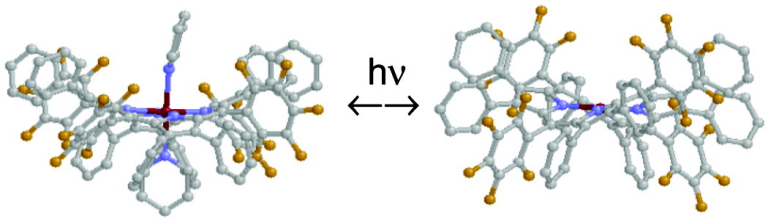

More About This Article

J|A|C|S
ARTICLES
Published on Web 07/19/2003

Photoinduced Axial Ligation and Deligation Dynamics of Nonplanar Nickel Dodecaarylporphyrins

Jennifer L. Retsek,[1a] Charles Michael Drain,[1b] Christine Kirmaier,[1a] Daniel J. Nurco,[1c] Craig J. Medforth,[1c,d] Kevin M. Smith,[1c,e] Igor V. Sazanovich,[1a,f] Vladimir S. Chirvony,[1f] Jack Fajer,[1g] and Dewey Holten*,[1a]

Contribution from the Department of Chemistry, Washington University, St. Louis, Missouri 63130, Hunter College and The Rockefeller University, New York, New York 10021, Department of Chemistry, University of California, Davis, California 95616, Biomolecular Materials and Interfaces Department, Sandia National Laboratories, Albuquerque, New Mexico 87185, Department of Chemistry, Louisiana State University, Baton Rouge, Louisiana 70803, Institute of Molecular and Atomic Physics, National Academy of Sciences of Belarus, F. Skaryna Avenue 70, Minsk, 220072, Belarus, and Materials Science Department, Brookhaven National Laboratory, Upton, New York 11973

Received April 29, 2002; E-mail: holten@wuchem.wustl.edu

Abstract: The ground- and excited-state metal−ligand dynamics of nonplanar nickel(II) 2,3,5,7,8,10,12,-13,15,17,18,20-dodecaphenylporphyrin (NiDPP) and two fluorinated analogues (NiF_{20}DPP and NiF_{28}DPP) have been investigated using static and time-resolved absorption spectroscopy in toluene and in ligating media that differ in basicity, aromaticity, and steric encumbrance. Because of the electronic and steric consequences of nonplanarity, NiDPP does not bind axial ligands in the ground state, but metal coordination does occur after photoexcitation with multistep dynamics that depend on the properties of the ligand. Following the structural relaxations that occur in all nickel porphyrins within ~10 ps, ligand binding to photoexcited NiDPP is progressively longer in pyridine, piperidine, and 3,5-lutidine (25−100 ps) but does not occur at all in 2,6-lutidine in which the ligating nitrogen is sterically encumbered. The transient intermediate that is formed, which nominally could be either a five- or six-coordinate species, also has a ligand-dependent lifetime (200−550 ps). Decay of this intermediate occurs partially via ligand release to re-form the uncoordinated species, in competition with binding of the second axial ligand and/or conformational/electronic relaxations (of a six-coordinate intermediate) to give the ground state of the bis-ligated photoproduct. The finding that the photoproduct channel principally depends on ligand characteristics along with the time-evolving spectra suggests that the transient intermediate may involve a five-coordinate species. In contrast to NiDPP, the fluorinated analogues NiF_{20}DPP and NiF_{28}DPP do coordinate axial ligands in the ground state but eject them after photoexcitation. Collectively, these results demonstrate the sensitivity with which the electronic and structural characteristics of the macrocycle, substituents, and solvent (ligands) can govern the photophysical and photochemical properties of nonplanar porphyrins and open new avenues for exploring photoinduced ligand association and dissociation behavior.

Introduction

Nickel(II) porphyrins are one of the most widely studied classes of metalloporphyrins. In the absence of axial ligands, the orbitals of the d^8 metal ion are filled through d_{z^2} with $d_{x^2-y^2}$ remaining empty. This is referred to as the $Ni(d_{z^2})^2$ metal ground-state configuration. Since the electronic absorption is dominated by the porphyrin ring (P), photoexcitation produces the macrocycle's lowest excited $^1(\pi,\pi^*)$ state (P*), with the metal remaining in the $(d_{z^2})^2$ configuration (left side of Figure 1). The state P* is nonfluorescent[2] because it decays in <1 ps[3−5] by internal conversion in which energy flows from the macrocycle to the metal[2−9] (process *a* in Figure 1). This results in the return of the macrocycle to its ground state and the promotion of a d_{z^2} electron to the $d_{x^2-y^2}$ orbital to produce the $^1(d_{z^2},d_{x^2-y^2})$ metal excited-state configuration, denoted $Ni^*(d_{z^2},d_{x^2-y^2})$. Since the $P^*Ni(d_{z^2})^2 \rightarrow PNi^*(d_{z^2},d_{x^2-y^2})$ process is downhill by ≥1 eV,[2b] the molecule is left with considerable excess electronic energy that must be converted to vibrational degrees of freedom. The composite vibrational-energy redistribution and flow to the solvent takes several to tens of picoseconds,[3−5,9] as is the case following ultrafast nonradiative decay in a number of porphyr-

(1) (a) Washington University. (b) Hunter College and The Rockefeller University. (c) University of California. (d) Sandia National Laboratories. (e) Louisiana State University. (f) National Academy of Sciences of Belarus. (g) Brookhaven National Laboratory.

(2) (a) Eastwood, D.; Gouterman, M. *J. Mol. Spectrosc.* **1970**, *35*, 359. (b) Antipas, A.; Gouterman, M. *J. Am. Chem. Soc.* **1983**, *105*, 4896.
(3) (a) Rodriguez, J.; Holten, D. *J. Chem. Phys.* **1989**, *91*, 3525. (b) Rodriguez, J.; Holten, D. *J. Chem. Phys.* **1990**, *92*, 5945.
(4) (a) Drain, C. M.; Kirmaier, C.; Medforth, C. J.; Nurco, D. J.; Smith, K. M.; Holten, D. *J. Phys. Chem.* **1996**, *100*, 11984. (b) Drain, C. M.; Gentemann, S.; Roberts, J. A.; Nelson, N. Y.; Medforth, C. J.; Jia, S.; Simpson, M. C.; Smith, K. M.; Fajer, J.; Shelnutt, J. A.; Holten, D. *J. Am. Chem. Soc.* **1998**, *120*, 3781.

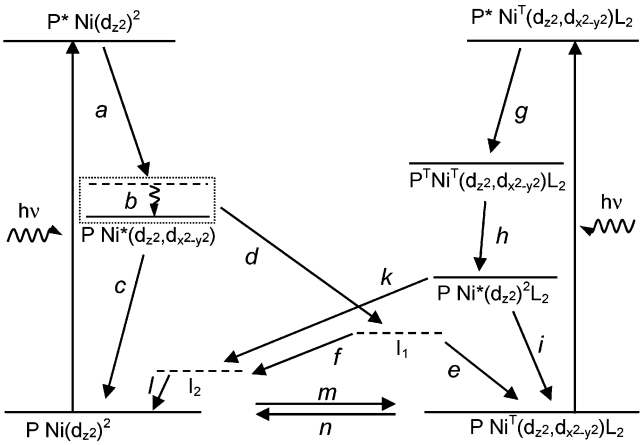

Figure 1. Schematic state diagram illustrating the key photoprocesses for photoexcited nickel porphyrins.

ins.[10] Additionally, population of the $d_{x^2-y^2}$ orbital (the lobes of which point at porphyrin-nitrogen lone pairs) causes electron−electron repulsion that must be relieved by structural rearrangements, including possible nonplanar distortions.[3,8−10] As a result of both the excess energy and electron repulsions, rapid P*Ni-$(d_{z^2})^2$ → PNi*(d_{z^2},$d_{x^2-y^2}$) internal conversion is followed by vibrational/conformational relaxation in the metal excited state (process *b* in Figure 1), which manifests as spectral shifts and wavelength-dependent kinetics on the time scale of tens of picoseconds.[3,4] Subsequent PNi*(d_{z^2},$d_{x^2-y^2}$) → PNi(d_{z^2}) deactivation (process *c* in Figure 1) occurs in 200−400 ps for planar nickel porphyrins such as nickel(II) 5,10,15,20-tetraphenylporphyrin (NiTPP) and nickel(II) 2,3,7,8,12,13,17,18-octaethylporphyrin (NiOEP, see Scheme 1).[3,6−12]

Nominally planar nickel porphyrins can bind two axial ligands to form six-coordinate adducts, with the extent of binding depending on both the porphyrin and the ligand.[13,14] For example, about 90% of the NiTPP molecules in neat piperidine (pip) are bis-ligated in the ground electronic state.[13,14] Evidence of singly ligated, five-coordinate intermediates has rarely been found.[3b,13,15] The ligands (L) sufficiently destabilize the d_{z^2} orbital such that an electron is promoted to the $d_{x^2-y^2}$ orbital, so that the metal ground state now has the $^3(d_{z^2},d_{x^2-y^2})$ configuration, referred to as $Ni^T(d_{z^2},d_{x^2-y^2})L_2$. Photoexcitation of a six-coordinate complex first produces the porphyrin $^1(\pi,\pi^*)$ state, with the metal remaining in the $^3(d_{z^2},d_{x^2-y^2})$ configuration; this excited state is denoted $P^*Ni^T(d_{z^2},d_{x^2-y^2})L_2$ (right side of Figure 1). On the time scale of just a few picoseconds, $P^*Ni^T(d_{z^2},d_{x^2-y^2})L_2$ decays and the PNi(d_{z^2})^2 ground state of the four-coordinate unligated nickel porphyrin forms. This extremely rapid conversion involves several intermediates, the first of which is likely $P^TNi^T(d_{z^2},d_{x^2-y^2})L_2$, which involves the macrocycle $^3(\pi,\pi^*)$ and metal $^3(d_{z^2},d_{x^2-y^2})$ configurations (process *g* in Figure 1).[3b,6c,d,16] Subsequent decay of this state produces the PNi*(d_{z^2})$^2L_2$ metal excited state (process *h*), which has a metal configuration unfavorable for the coordinated ligands. Thus, both ligands are rapidly released (process *k*). Whether both ligands are ejected simultaneously is unclear, and some deactivation competing with ligand release may occur (process *i*). In a simplistic scheme (Figure 1), ligand release may involve a transient five-coordinate intermediate I_2, or I_2 may be the four-coordinate species that relaxes further via vibrational/conformational equilibration. Such scenarios have been discussed in the literature in view of scant evidence for a five-coordinate intermediate.[3b,9c,17] The subsequent rebinding of the ligands to give the original $PNi^T(d_{z^2},d_{x^2-y^2})L_2$

Scheme 1. Structure and Nomenclature of Substituted Nickel Porphyrins and Solvents

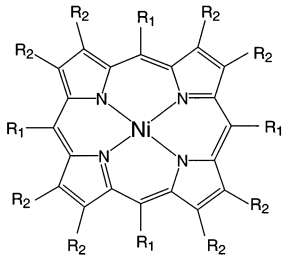

Compound	R_1	R_2
NiDPP	$-C_6H_5$	$-C_6H_5$
NiF_{20}DPP	$-C_6F_5$	$-C_6H_5$
NiF_{28}DPP	$-C_6F_5$	$-C_6H_4F$
NiOETPP	$-C_6H_5$	$-C_2H_5$
NiTPP	$-C_6H_5$	-H
NiOEP	-H	$-C_2H_5$

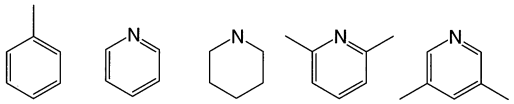

toluene pyridine piperidine 2,6-lutidine 3,5-lutidine

(5) Eom, H. S.; Jeoung, S. C.; Kim, D.; Ha, J.-H.; Kim, Y.-R. *J. Phys. Chem. A* **1997**, *101*, 3661.
(6) (a) Kobayashi, T.; Straub, K. D.; Rentepis, P. M. *Photochem. Photobiol.* **1979**, *29*, 925. (b) Chirvonyi, V. S.; Dzhagarov, B. M.; Timinskii, Y. V.; Gurinovich, G. P. *Chem. Phys. Lett.* **1980**, *70*, 79. (c) Chivonyi, V. S.; Dzhagarov, B. M.; Shul′ga, M.; Gurinovich, G. P. *Dokl. Akad. Nauk. SSSR* **1981**, *259*, 144. (d) Dzhagarov, B. M.; Chirvonyi, V. S.; Gurinovich, G. P. In *Laser Picosecond Spectroscopy and Photochemistry of Biomolecules*; Letokhov, V. S., Ed.; Hilger: Bristol, 1987; p 137.
(7) (a) Kim, D.; Kirmaier, C.; Holten, D. *Chem. Phys.* **1983**, *75*, 305. (b) Kim, D.; Holten, D. *Chem. Phys. Lett.* **1983**, *98*, 584.
(8) (a) Findsen, E.; Shelnutt, J. A.; Friedman, J. A.; Ondrias, M. *Chem. Phys. Lett.* **1986**, *126*, 465. (b) Courtney, S. H.; Jedju, T. M.; Friedman, J. M.; Alden, R. G.; Ondrias, M. R. *Chem. Phys. Lett.* **1989**, *164*, 39.
(9) (a) Kruglik, S. G.; Mizutani, Y.; Kitagawa, T. *Chem. Phys. Lett.* **1997**, *266*, 283. (b) Uesugi, Y.; Mizutani, Y.; Kitagawa, T. *J. Phys. Chem. A* **1998**, *102*, 5809. (c) Kruglik, S. G.; Ermolenkov, V. V.; Orlovich, V. A.; Turpin, P.-Y. *Chem Phys.* **2003**, *286*, 97.
(10) (a) Rodriguez, J.; Kirmaier, C.; Holten, D. *J. Am. Chem. Soc.* **1989**, *111*, 6300. (b) Bilsel, O.; Rodriguez, J.; Holten, D. *J. Phys. Chem.* **1990**, *94*, 3508. (c) Bilsel, O.; Milam, S. N.; Girolami, G. S.; Suslick, K. S.; Holten, D. *J. Phys. Chem.* **1993**, *97*, 7216.
(11) (a) Chikisev, A. Y.; Kamalov, V. F.; Korteev, N. I.; Kvach, V. V.; Shkvrinov, A. P.; Toluetaev, B. N. *Chem. Phys. Lett.* **1988**, *144*, 90. (b) Apanasevich, P. A.; Kvach, V. V.; Orlovich, V. A. *J. Raman Spectrosc.* **1989**, *20*, 125. (c) Sato, S.; Kitiagawa, T. *Appl. Phys.* **1994**, *B59*, 415.
(12) Given the speed of these events, the photophysical processes for the four-coordinate nickel porphyrins likely involve only states in the singlet manifold (left side of Figure 1),[3,10a] although involvement of $^3(d_{z^2}, d_{x^2-y^2})$ has been discussed.[6,7]
(13) Jia, S.-L.; Jentzen, W.; Shang, M.; Song, X.-Z.; Ma, J.-G.; Scheidt, W. R.; Shelnutt, J. A. *Inorg. Chem.* **1998**, *37*, 4402.
(14) (a) The extent of binding of two ligands to a nickel porphyrin depends on the strength of the Lewis base ligand and the acidity of the porphyrin's central nickel ion, the latter being modulated by the nature and location of the peripheral substituents on the macrocycle. Five-coordinate nickel porphyrins are rarely observed. The metal ion for NiTPP is more acidic than that of NiOEP[14b] causing ligand binding to be more extensive for the former porphyrin. For example, in the electronic ground state, NiTPP is approximately 90% six-coordinate in piperidine, whereas NiOEP is only ∼75% coordinated.[3b,7] In the weaker base pyridine, NiTPP is only ∼40% coordinated, while NiOEP remains essentially unligated.[3b,7] (b) For NiTPP, the central nitrogens to which the metal is bound as well as the *meso* carbons to which the phenyl groups are bound both have considerable electron density in the $a_{2u}(\pi)$ HOMO. On the other hand, the β carbons to which ethyl groups of NiOEP are attached have electron density in the $a_{1u}(\pi)$ orbital, which has negligible density at the central nitrogens and thus the central metal.[14c] (c) Gouterman, M. In *The Porphyrins*; Dolphin, D., Ed.; Academic: New York, 1978; Vol. III, pp 1−153.
(15) Kim, D.; Su, Y. O.; Spiro, T. G. *Inorg. Chem.* **1986**, *25*, 3988.

ground state is comparatively slow (involving electronic, nuclear, and spin changes), taking tens to hundreds of nanoseconds (process *m*).[6c,d,18] The photodissociation process for $NiTPP(pip)_2$ has been studied by nanosecond, time-resolved EXAFS spectroscopy, supporting this basic framework.[19]

Ligand binding by photoexcited four-coordinate nickel porphyrins is also a readily observed phenomenon.[7,9b,c] A notable example of this behavior is displayed by NiOEP in pyridine, where the porphyrin is essentially unligated in the ground state. Excitation of NiOEP in pyridine produces the $P^*Ni(d_{z^2})^2$ macrocycle excited state followed by <1 ps internal conversion to the $PNi^*(d_{z^2},d_{x^2-y^2})$ metal excited state, as is the case in nonligating solvents (process *a* in Figure 1). However, the $(d_{z^2},d_{x^2-y^2})$ metal configuration is associative toward the available pyridine ligands, which are bound in an overall process that also involves a change of spin and (probably) conformational/vibrational relaxation in order to produce the $PNi^T(d_{z^2},d_{x^2-y^2})L_2$ ground state of the six-coordinate adduct. This conversion is simplified as processes *d* and *e* in Figure 1, where a putative transient intermediate I_1 is indicated. Simple models for I_1 are that it is a five-coordinate species, or that it is a vibrationally/structurally unrelaxed form of the six-coordinate species. No matter the model, spectral or kinetic resolution of the formation and decay of any intermediate between the $PNi^*(d_{z^2},d_{x^2-y^2})$ metal excited state and $PNi^T(d_{z^2},d_{x^2-y^2})L_2$ has not been clearly demonstrated to date for the planar porphyrins. Subsequent ligand loss and the associated electronic/structural changes to re-form the original unligated $PNi(d_{z^2})^2$ ground state are again comparatively slow and occur on the nanosecond time scale (process *n*).

In contrast to the extensive studies of the excited-state dynamics of the planar nickel porphyrins, there have been relatively few studies of nonplanar nickel porphyrins. Such studies are of interest because nonplanar free base and zinc porphyrins show dramatic differences in photophysical properties compared to their planar analogues.[20−24] These differences are thought to arise in part from multiple conformations being energetically accessible in the both ground and excited electronic states (conformational flexibility) and a propensity for photoinduced conformational changes.[20−24] For example, although unligated ruffled[25] nickel(II) 2,3,5,7,8,10,12,13,15,17,18,20-dodecaphenylporphyrin (NiDPP, Scheme 1) shows the same basic deactivation pathways as planar NiTPP (processes *a*, *b*, *c* in Figure 1), the spectral and kinetic data are much more complex and show a strong dependence on solvent viscosity and temperature.[4a] These observations have been ascribed to presence of multiple accessible conformations and enhanced excursions among these configurations following excitation. Unligated, ruffled,[4b] nickel(II) tetra-*tert*-butylporphyrin [NiT(t-Bu)P, Scheme 1] shows even more novel behavior in that the lifetime of the $PNi^*(d_{z^2},d_{x^2-y^2})$ metal excited state (process *c* in Figure 1) varies by over 6 orders of magnitude (picoseconds to microseconds) as a function of temperature and dielectric properties of the solvent, whereas the lifetime for planar NiTPP is virtually constant.[4b] This behavior is ascribed to the metal excited state adopting an asymmetric, polar nonplanar configuration and the need for the system to surmount conformational barriers en route to the electronic/structural ground state.

In view of these findings, one might expect that the axial-ligation behavior of nonplanar nickel porphyrins would also show characteristics that differ from those for the planar molecules. To this end, we have utilized ultrafast optical spectroscopy to investigate the photoinduced binding/release of nitrogenous bases from NiDPP, nickel(II) 2,3,7,8,12,13,17,18-octaphenyl-5,10,15,20-tetrakis(pentafluorophenyl)porphyrin (NiF_{20}DPP) and nickel(II) 2,3,7,8,12,13,17,18-octakis(4-fluorophenyl)-5,10,15,20-tetrakis(pentafluorophenyl)porphyrin (NiF_{28}DPP, Scheme 1). Evidence for the conformational flexibility of these molecules comes from X-ray crystal structures. NiDPP, NiF_{20}DPP, and NiF_{28}DPP as well as the bis-pyridine adducts $NiF_{20}DPP(pyr)_2$ and $NiF_{28}DPP(pyr)_2$ can crystallize in more than one conformation involving differing degrees of saddle and ruffle distortions (Figure 2).[25,26,27] This series of nickel porphyrins may be expected to show differences in photoinduced axial-ligation dynamics from one another deriving from the interrelated structural, electronic, and solvent-interaction effects of the peripheral substituents (e.g., fluorinated phenyl rings), in analogy to the properties we recently found for the free base and zinc-

(16) The $P^TNi^T(d_{z^2})^2L_2$ state has three sublevels, a singlet, a triplet, and a quintet, with internal conversion from the macrocycle excited-state $P^*Ni^T(d_{z^2}, d_{x^2-y^2})L_2$ to the triplet form being spin allowed, consistent with the observed fast decay of the $P^*Ni^T(d_{z^2}, d_{x^2-y^2})L_2$ decay.[3b]

(17) Vibrational relaxation dynamics may be convolved with the evolution of the short-lived intermediates prior to the deligation step (not indicated in Figure 1).[3b,7]

(18) Hoshino, M. *Inorg. Chem.* **1986**, *25*, 2476.

(19) Chen, L. X.; Jäger, W. J. H.; Jennings, G.; Gosztola, D. J.; Munkholm, A.; Hessler, J. P. *Science* **2001**, *292*, 262.

(20) (a) Barkigia, K. M.; Berber, M. D.; Fajer, J.; Medforth, C. J.; Renner, M. W.; Smith, K. M. *J. Am. Chem. Soc.* **1990**, *112*, 8851. (b) Shelnutt, J. A.; Medforth, C. J.; Berber, M. D.; Barkigia, K. M.; Smith, K. M. *J. Am. Chem. Soc.* **1991**, *113*, 4077. (c) Charlesworth, P.; Truscott, T. G.; Kessel, D.; Medforth, C. J.; Smith, K. M. *J. Chem. Soc., Faraday Trans.* **1994**, *90*, 1073. (d) Jentzen, W.; Simpson, M. C.; Hobbs, J. D.; Song, X.; Ema, T.; Nelson, N. Y.; Medforth, C. J.; Smith, K. M.; Veyrat, M.; Mazzanti, M.; Ramasseul, R.; Marchon, J.-C.; Takeuchi, T.; Goddard, W. A.; III; Shelnutt, J. A. *J. Am. Chem. Soc.* **1995**, *117*, 11085. (e) Shelnutt, J. A.; Song, X. Z.; Ma, J.-G.; Jia, S. L.; Jentzen, W.; Medforth, C. J. *Chem. Soc. Rev.* **1998**, *27*, 31. (f) Haddad, R. E.; Gazeau, S.; Pecaut, J.; Marchon, J.-C.; Medforth, C. J.; Shelnutt, J. A. *J. Am. Chem. Soc.* **2003**, *124*, 1253.

(21) (a) Takeda, J.; Ohya, T.; Sato, M. *Chem. Phys. Lett.* **1991**, *183*, 384. (b) Ravikanth, M.; Chandrashekar, T. K. *Struct. Bond.* **1995**, *82*, 105. (c) DiMagno, S. G.; Wertsching, A. K.; Ross, C. R., II *J. Am. Chem. Soc.* **1995**, *117*, 829. (d) Parusel, A. B. J.; Wondimagegn, T.; Ghosh, A. *J. Am. Chem. Soc.* **2000**, *122*, 6371. (e) Sminov, V. V.; Woller, E. K.; Tatman, D.; DiMagno, S. G. *Inorg. Chem.* **2001**, *40*, 2614. (f) Wertsching, A. K.; Koch, A. S.; DiMagno, S. G. *J. Am. Chem. Soc.* **2001**, *123*, 3932. (g) Ryeng, H.; Gosh, A. *J. Am. Chem. Soc.* **2002**, *124*, 8099.

(22) (a) Gentemann, S.; Medforth, C. J.; Forsyth, T. P.; Nurco, D. J.; Smith, K. M.; Fajer, J.; Holten, D. *J. Am. Chem. Soc.* **1994**, *116*, 7363. (b) Gentemann, S. G.; Nelson, N. Y.; Jaquinod, L. A.; Nurco, D. J.; Leung, S. H.; Smith, K. M.; Fajer, J.; Holten, D. *J. Phys. Chem. B* **1997**, *101*, 1247.

(23) (a) Chirvony, V. S.; van Hoek, A.; Galievsky, V. A.; Sazanovich, I. V.; Schaafsma, T. J.; Holten, D. *J. Phys. Chem. B* **2000**, *104*, 9909. (b) Sazanovich, I. V.; Galievsky, V. A.; van Hoek, A.; Schaafsma, T. J.; Malinovskii, V. L.; Holten, D.; Chirvony, V. S. *J, Phys. Chem. B* **2001**, *105*, 7818.

(24) (a) Retsek, J. L.; Medforth, C. J.; Nurco, D. J.; Gentemann, S.; Chirvony, V. S.; Smith, K. M.; Holten, D. *J. Phys. Chem. B* **2001**, *105*, 6396. (b) Retsek, J. L.; Gentemann, S.; Medforth, C. J.; Smith, K. M.; Chirvony, V. S.; Fajer, J.; Holten, D. *J. Phys. Chem. B* **2000**, *104*, 6690.

(25) (a) Barkigia, K. M.; Renner, M. W.; Furenlid, L. R.; Medforth, C. J.; Smith, K. M.; Fajer, J. *J. Am. Chem. Soc.* **1993**, *115*, 3627. (b) Nurco, D. J.; Medforth, C. J.; Forsyth, T. P.; Olmstead, M. M.; Smith, K. M. *J. Am. Chem. Soc.* **1996**, *118*, 10918. (c) Barkigia, K. M.; Nurco, D. J.; Renner, M. W.; Melamed, D.; Smith, K. M.; Fajer, J. *J. Phys. Chem. B* **1998**, *102*, 322.

(26) (a) Nurco, D. J.; Smith, K. M.; Fajer, J. Unpublished results. (b) Nurco, D. J. Ph.D. Dissertation Thesis, University of California, 1998. (c) The structure of $NiF_{20}(pyrrolidine)_2$ has also been solved and this complex adopts a saddle structure with some ruffle distortion.

(27) The nomenclature for nonplanar distortions is that suggested by Scheidt and Lee (Scheidt, W.; Lee, Y. J. *Struct. Bonding (Berlin)*, **1987**, *64*, 1.) In a saddle conformation, alternate pyrrole rings are tilted up and down with respect to a least-squares plane through the 24 atoms of the porphyrin core and the *meso* carbon atoms lie in the least-squares plane. In a ruffled conformation, alternate pyrrole rings are twisted clockwise or counterclockwise about the metal-nitrogen bond and the *meso* carbon atoms are alternately above or below the least-squares plane through the 24 atoms of the porphyrin core.

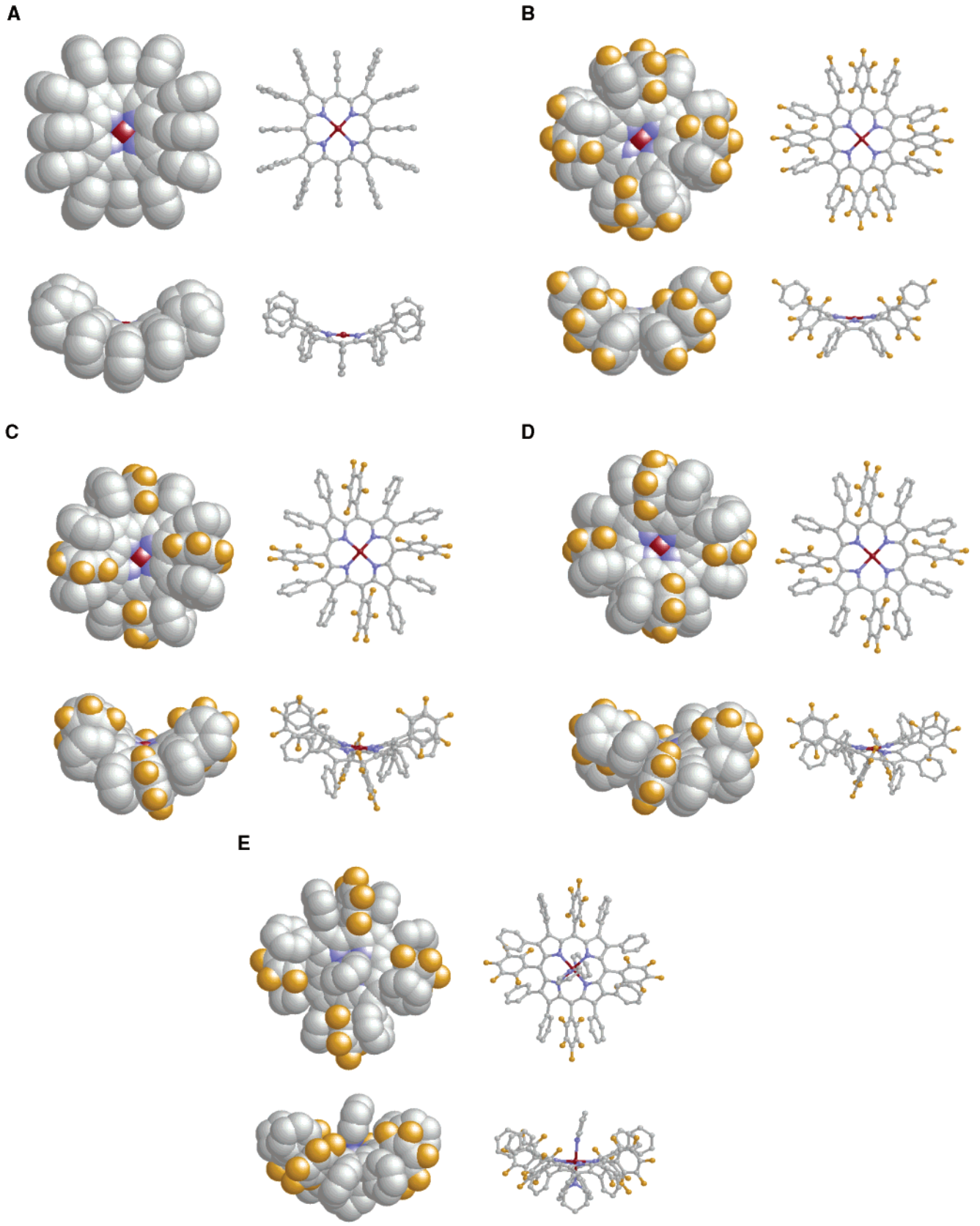

Figure 2. Structures for representative nonplanar porphyrins showing top and side views in space-filling and ball-and-stick representations: ruffled NiDPP (a), saddle-shaped $NiF_{28}DPP$ (b), $NiF_{20}DPP$ with different degrees of saddle and ruffle distortions (c and d), and $NiF_{20}DPP(pyridine)_2$ with a saddle structure having minor ruffle distortions (e). The data are taken from refs 25b,c and 26.

(II) analogues (e.g., H_2DPP, $H_2F_{20}DPP$, ZnDPP, $ZnF_{20}DPP$).[24] Indeed, we find that these nonplanar nickel porphyrins show differences from one another in ground- and excited-state ligation properties as well as behaviors not seen previously for

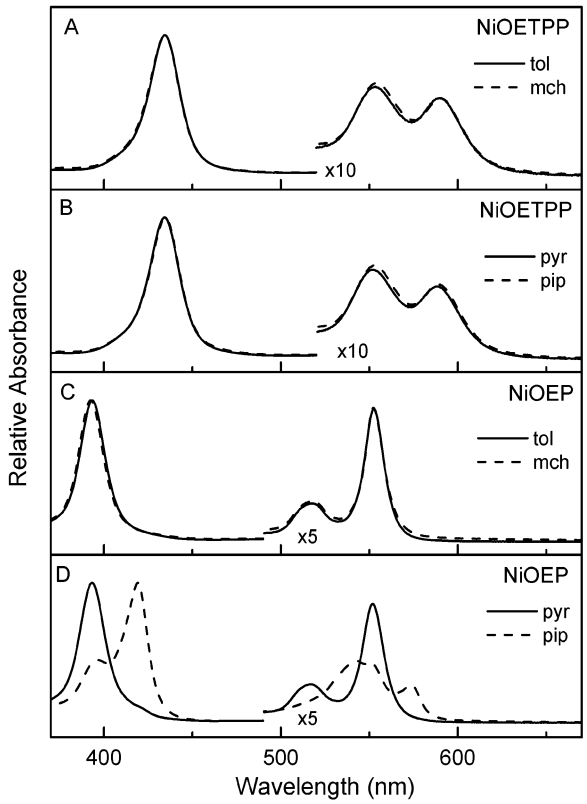

Figure 3. Room-temperature ground-state absorption spectra for nonplanar NiOETPP and nominally planar NiOEP in toluene (tol), methylcyclohexane (mch), pyridine (pyr), and piperidine (pip).

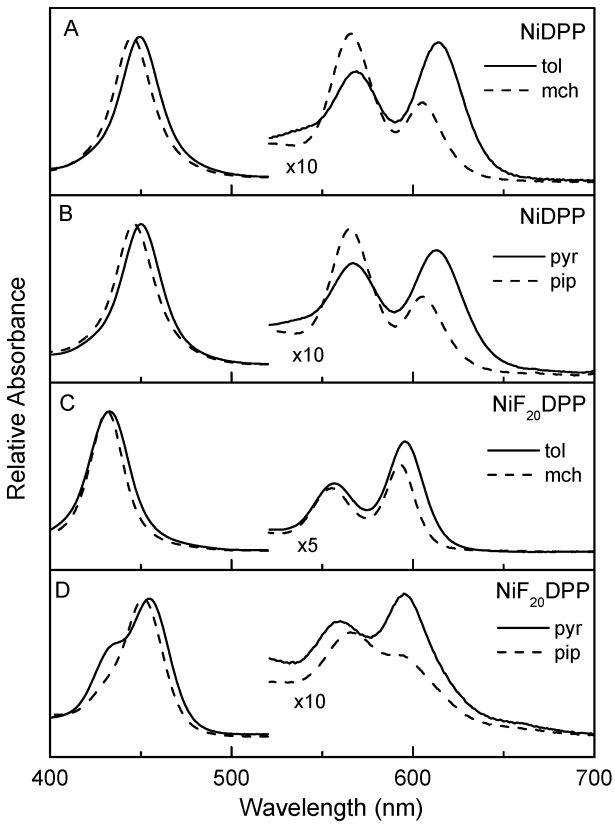

Figure 4. Room-temperature ground-state absorption spectra for nonplanar NiDPP and $NiF_{20}DPP$ in toluene (tol), methylcyclohexane (mch), pyridine (pyr), and piperidine (pip).

planar analogues. These results clearly demonstrate the considerable effect of macrocycle nonplanarity on axial ligation/deligation energetics and dynamics and further extend the increasing body of data on the often-dramatic consequences of conformational distortions and the associated electronic readjustments on the chemical and photophysical properties of porphyrins.

Experimental Section

The compounds (Scheme 1) nickel(II) 2,3,5,7,8,10,12,13,15,17,18,-20-dodecaphenylporphyrin (NiDPP),[28a] nickel(II) 2,3,7,8,12,13,17,18-octaphenyl-5,10,15,20-tetrakis(pentafluorophenyl)porphyrin (NiF_{20}-DPP),[28b] nickel(II) 2,3,7,8,12,13,17,18-octakis(4-fluorophenyl)-5,10,15,20-tetrakis(pentafluorophenyl)porphyrin ($NiF_{28}DPP$),[28b] and nickel(II) 2,3,7,8,12,13,17,18-octaethyl-5,10,15,20-tetraphenylporphyrin (NiOETPP)[20b] were synthesized as described previously. NiOEP was purchased from Porphyrin Products (Logan, UT). Ground-state absorption spectra were collected at room temperature on a Cary 100 UV−visible spectrophotometer using 2−5 μM samples. All solvents employed were either spectrophotometric or HPLC grade. Transient absorption measurements were carried out on either of two instruments described previously, using 130 fs, 35−40 μJ excitation pulses from a Ti:sapphire/OPA-based laser system or 200 fs, 0.2 mJ pump pulses at 582 nm from an amplified sync-pumped dye-laser-based system.[29] In some cases, experiments were performed on both instruments, with identical results being obtained. Both spectrometers used white-light probe pulses of duration comparable to the excitation flashes and samples (25−50 μM) in 2-mm path length cuvettes at room temperature. Because of dispersion in the arrival times of the various wavelengths in the white-light probe pulse at the sample, spectra shown at <1 ps were each constructed from several spectra acquired at the appropriate successive pump−probe delay settings. Slower time-scale experiments were carried out on a conventional flash-photolysis setup utilizing 5-ns excitation flashes at 532 nm.[22]

Results

Ground-State Absorption Spectra. Absorption spectra of saddle-shaped[25a] NiOETPP and nominally planar[30] NiOEP are shown in Figure 3. Spectra of the nonplanar porphyrins NiDPP and $NiF_{20}DPP$, which are the principal focus of this study, are shown in Figure 4. All of these nickel porphyrins display a strong near-UV Soret band (390−460 nm), corresponding to absorption to the macrocycle's second $^1(\pi,\pi^*)$ excited state and weaker Q(1,0) and Q(0,0) bands (520−620 nm), corresponding to transitions to the macrocycle's lowest $^1(\pi,\pi^*)$ excited state (P* in Figure 1). For NiOEP these three bands are at approximately 395, 515, and 550 nm in both toluene and methylcyclohexane, neither of which is capable of coordinating to the central nickel ion (Figure 3C). The same is true for NiOEP in pyridine, indicating that coordination of this nitrogenous base to the nickel ion does not occur to any measurable degree (Figure 3D, solid line). On the other hand, a large fraction

(28) (a) Medforth, C. J.; Senge, M. O.; Smith, K. M.; Sparks, L. D.; Shelnutt, J. A. *J. Am. Chem. Soc.* **1992**, *114*, 9859. (b) Kadish, K. M.; Lin, M.; Van Caemelbecke, E.; De Stefano, G.; Medforth, C. J.; Nurco, D. J.; Nelson, N. Y.; Krattinger, B.; Muzzi, C. M.; Jaquinod, L.; Xu, Y.; Shyr, D. C.; Smith, K. M.; Shelnutt, J. A. *Inorg. Chem.* **2002**, *41*, 6673.

(29) (a) Yang, S. I.; Lammi, R. K.; Seth, J.; Riggs, J. A.; Arai, T.; Kim, D.; Bocian, D. F.; Holten, D.; Lindsey, J. S. *J. Phys. Chem. B* **1998**, *102*, 9426. (b) Kirmaier, C.; Weems, D.; Holten, D. *Biochemistry* **1999**, *38*, 11516.

(30) (a) Alden, R. G.; Crawford, B. A.; Doolen, R.; Ondrias, M. R.; Shelnutt, J. A. *J. Am. Chem. Soc.* **1989**, *111*, 2070. (b) Brennan, T. D.; Scheidt, W. R.; Shelnutt, J. A. *J. Am. Chem. Soc.* **1988**, *110*, 3913. (c) Cullen, D. L.; Meyer, E. F. *J. Am. Chem. Soc.* **1974**, *96*, 2095. (d) Meyer, E. F. *Acta Crystallogr.* **1972**, *B28*, 2162.

(~75%) of the NiOEP molecules in the stronger base piperidine is in the six-coordinate, bis-axially coordinated form (Figure 3D, dashed line).[7] This ligand binding is evidenced by the new Soret and Q(1,0) and Q(0,0) features in addition to those derived from the fraction of the molecules that remain in the four-coordinate, unligated form. The absorption bands of the ligated complex display the classic ~25 nm red shift from the positions for the uncoordinated porphyrin, and the ratio of the Q-bands is reversed.

The spectra of NiOETPP in toluene and methylcyclohexane are also identical to one another, but are red-shifted relative to NiOEP as a result of the nonplanar distortions (Figure 3A).[25a] Unlike NiOEP, the spectra of NiOETPP in both pyridine and piperidine are identical to those in the noncoordinating solvents, indicating that neither ligand binds to this nonplanar porphyrin (Figure 3B).[20b] NiDPP has phenyl rather than ethyl groups at the eight β pyrrole positions (Scheme 1) and adopts (at least in the crystal structures) ruffle and mixed ruffle/saddle structures as compared to the saddle conformation of NiOETPP.[25b,c,27] The spectra for NiDPP in toluene and methylcyclohexane are different from one another, both in the positions of the bands and in the ratio of the Q-bands (Figure 4A). The spectral differences in these two nonpolar, noncoordinating solvents suggest that the aromatic character of toluene allows specific solute−solvent interactions such as π-stacking with the peripheral phenyl rings and/or macrocycle of NiDPP that are not possible for methylcyclohexane. This view is supported by the analogous spectral difference for NiDPP in aromatic pyridine and its nonaromatic counterpart piperidine (Scheme 1 and Figure 4B). Furthermore, the fact that the spectra in pyridine and toluene are virtually identical to one another and that the same is true for piperidine and methylcyclohexane indicates that the nitrogenous-base solvent molecules do not measurably coordinate to NiDPP, similar to the absence of ligand binding to NiOETPP.[20b]

The four *meso*-phenyl rings of NiDPP are replaced by pentafluorophenyl groups in NiF_{20}DPP, which adopts saddle and mixed saddle/ruffle conformations.[25b,26b] The spectrum of NiF_{20}DPP in methylcyclohexane and toluene are similar, although not identical (Figure 4C), and generally blue-shifted compared to NiDPP. A general blue shift is observed for other fluorinated porphyrins (including ZnF_{20}DPP and ZnF_{20}TPP) and can be ascribed to the electron-withdrawing effects of the fluorinated phenyl rings on the energies and electron distributions of the highest occupied and lowest unoccupied molecular orbitals of the porphyrins.[31] Unlike NiDPP, NiF_{20}DPP does bind pyridine and piperidine ligands (Figure 4D). Two Soret bands are found in pyridine, one at the same position as in the noncoordinating solvents and one that is red-shifted by ~20 nm (Figure 4D solid line). This latter feature is undoubtedly due to the formation of the six-coordinate $NiF_{20}DPP(pyr)_2$ adduct, which has been shown by X-ray analysis to exhibit mainly saddle structures with varying degrees of ruffle distortions.[26] The integrated ratio of the two Soret features indicates that roughly 65% of the NiF_{20}DPP molecules are six-coordinate in pyridine, with the remainder in the four-coordinate, unligated form; the percentage of ligated molecules is ~80% in piperidine (Figure 4D, dashed line). The effect of ligand binding to NiF_{20}DPP on the Q-bands is much smaller than that found for the planar porphyrins such as NiOEP (compare Figures 3D and 4D). Ligand binding to NiF_{28}DPP is similar to that found for NiF_{20}DPP (data not shown). Evidently, the increase in metal acidity derived from the electron-withdrawing character of the fluorinated phenyl rings, and interrelated structural effects due to the change in substituents, serves to increase the ligand-binding ability of NiF_{20}DPP and NiF_{28}DPP compared to that of NiDPP and NiOETPP.

These results are consonant with a general trend noted for nonplanar porphinoids.[32a] Namely, as the macrocycle distorts, the porphyrin nitrogens move closer to the metal ion (as evidenced by shorter Ni−N distances[33]) and the associated change in the electrophilicity of the low-spin nickel lessens the tendency to bind axial ligands. Introducing electron-withdrawing groups, such as the multiple fluorinated phenyl rings of NiF_{20}DPP and NiF_{28}DPP, can restore the ligand affinity. These results demonstrate the counterbalancing structural and electron-withdrawing effects on the relative energies of the metal d_{z^2} and $d_{x^2-y^2}$ orbitals and thus the relative energies (and ease of formation) of the electronic configurations appropriate for the unligated and ligated forms, namely $(d_{z^2})^2$ and $(d_{z^2},d_{x^2-y^2})$, respectively. In the same vein, the peripherally crowded nonplanar nickel porphyrins have steric barriers toward ligand binding related to the larger nickel ion in the ligated, $(d_{z^2}, d_{x^2-y^2})$ form.[20b,32]

Transient Absorption Spectra and Kinetics. (a) NiDPP in Toluene. Representative Soret-region transient absorption difference spectra and kinetic data for NiDPP in toluene are shown in Figures 5A and 6A. The data are in excellent agreement with those obtained and analyzed in detail previously for NiDPP in this and other noncoordinating solvents.[4a] Therefore, only a summary of the results will be presented, using the state diagram on the left of Figure 1 and the associated description of the electronic configurations given in the Introduction. The spectrum observed immediately after excitation is characteristic of the lowest $^1(\pi,\pi^*)$ excited state (P*) of the porphyrin macrocycle[3,34] and is dominated by bleaching of the ground-state Soret band flanked by weak, featureless transient absorption (Figure 5A, solid line). The spectrum evolves within 2 ps into a derivative-type spectrum similar to that seen at 15 ps, but more asymmetric in form, and then over the next 10 ps or so to the more symmetric derivative shape seen at 15 ps (Figure 5A, dashed line). The derivative-shaped spectra can be assigned to the $(d_{z^2},d_{x^2-y^2})$ excited state of the metal, denoted $PNi^*(d_{z^2},d_{x^2-y^2})$ in Figure 1, and the spectral changes over the first 10 ps or so to the formation and vibrational/conformational relaxation of this state.[35] The relaxed $(d_{z^2},d_{x^2-y^2})$ excited state decays uniformly to the ground state by 300 ps (Figure 5A, dotted line).

(31) Yang, S. I.; Seth, J.; Strachan, J.-P.; Gentemann, S.; Kim, D.; Holten, D.; Lindsey, J. S.; Bocian, D. F. *J. Porphyrins Phthalocyanines* **1999**, *3*, 117.

(32) (a) Eschenmoser, A. *Ann N.Y. Acad. Sci.* **1986**, *471*, 108. (b) Barkigia, K. M.; Nelson, N. Y.; Renner, M. W.; Smith, K. M.; Fajer, J. *J. Phys. Chem. B.* **1999**, *41*, 8643. (c) Renner, M. W.; Barkigia, K. M.; Melamed, D.; Gisselbrecht, J.-P.; Nelson, N. Y.; Smith, K. M.; Fajer, J. *Res. Chem. Intermed.* **2002**, *28*, 741.

(33) The macrocycle Ni−N distances in the different conformers of NiDPP range between 1.885(6) and 1.909(5) Å,[25b,c] those for NiF_{20}DPP between 1.892(3) to 1.924(3) Å,[25b,26c] that for NiF_{28}DPP is 1.914(4) Å,[25b] while those for the ligated forms $NiF_{20}DPP(pyr)_2$ and $NiF_{28}DPP(pyr)_2$ lengthen significantly to 2.03−2.04 Å, with associated distances to the pyridines of 2.18−2.23 Å.[26]

(34) Rodriguez, J.; Kirmaier, C.; Holten, D. *J. Am. Chem. Soc.* **1989**, *111*, 6500.

(35) A derivative-shaped near-UV absorption-difference spectrum for a (d,d) excited state is consistent with the idea that the Soret (π,π^*) absorption band of the macrocycle will be shifted from the position in the ground electronic state due to the change in electron density at the metal. Whether the excited-state Soret band is blue or red shifted in the excited state will depend on electronic and structural differences with the ground state.

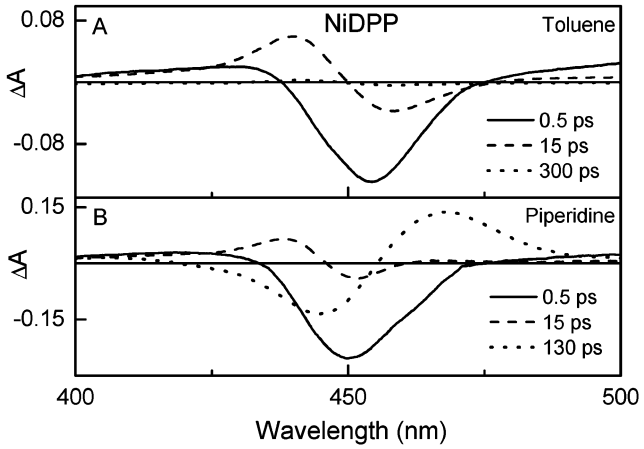

Figure 5. Soret-region transient absorption difference spectra at selected delay times for NiDPP in toluene (A) and piperidine (B) obtained at room temperature using 130-fs excitation flashes at 550 nm.

Representative kinetic data at 462 nm and fit to a three-exponential function (solid line) are shown in Figure 6A. As has been reported previously for NiDPP[4a] and planar nickel porphyrins[3,5] in noncoordinating solvents, the fit values (particularly for the first two kinetic components) vary significantly as a function of probing wavelength, reflective of the multiple processes/conformations/etc. that contribute. For example, between 420 and 460 nm the time constant of the fast component for NiDPP varies from 0.3 to 1.1 ps (average ~0.7 ps using single-wavelength and global analysis), the second varies from 3 to 12 ps (average ~7 ps), and the third is in the range 100−140 ps (average ~120 ps). The P*Ni$(d_{z^2})^2$ → PNi*$(d_{z^2},d_{x^2-y^2})$ internal conversion from the macrocycle to metal excited state (process *a* in Figure 1) likely has a time constant <1 ps since the initial kinetic phase overlaps the initial stages of vibrational/conformational relaxation in the metal PNi*$(d_{z^2},d_{x^2-y^2})$ excited state (process *b*), which is responsible for the middle kinetic phase that extends past 10 ps. The ~120 ps kinetic component represents the PNi*$(d_{z^2},d_{x^2-y^2})$ → PNi$(d_{z^2})^2$ metal excited state → ground state deactivation (process *c*).

(b) NiDPP in Piperidine. Difference spectra for NiDPP in piperidine at three key times following excitation are shown in Figure 5B; the spectral evolution is presented in more detail in Figure 7. Representative kinetic data at 447 nm and a fit to four exponentials plus a constant (long-time asymptote) are shown in Figure 6B. The average values of the time constants using single-wavelength and global analysis of the data between ~430 and 480 nm are ~0.7, ~3, ~65, and ~200 ps. The values vary with probe wavelength and like the early phases this is quite prominent for the fourth phase (100−400 ps); there may be an additional component on the time scale of tens of picoseconds. The data demonstrate the binding of piperidine ligands by photoexcited four-coordinate NiDPP as follows.

By analogy to the results in toluene (Figure 5A), the first two phases in piperidine involve evolution of an initial spectrum (Figures 5B and 7A, solid line) that can be assigned to the macrocycle (P*) excited state evolving to a derivative-shaped spectrum at 15 ps (Figure 5B, dashed line) due to the Ni*$(d_{z^2},d_{x^2-y^2})$ metal excited state of unligated NiDPP. In keeping with the interpretations given above for NiDPP in toluene, the data are readily ascribed to decay of the macrocycle P* excited state in <1 ps followed by conformational/vibrational relaxation

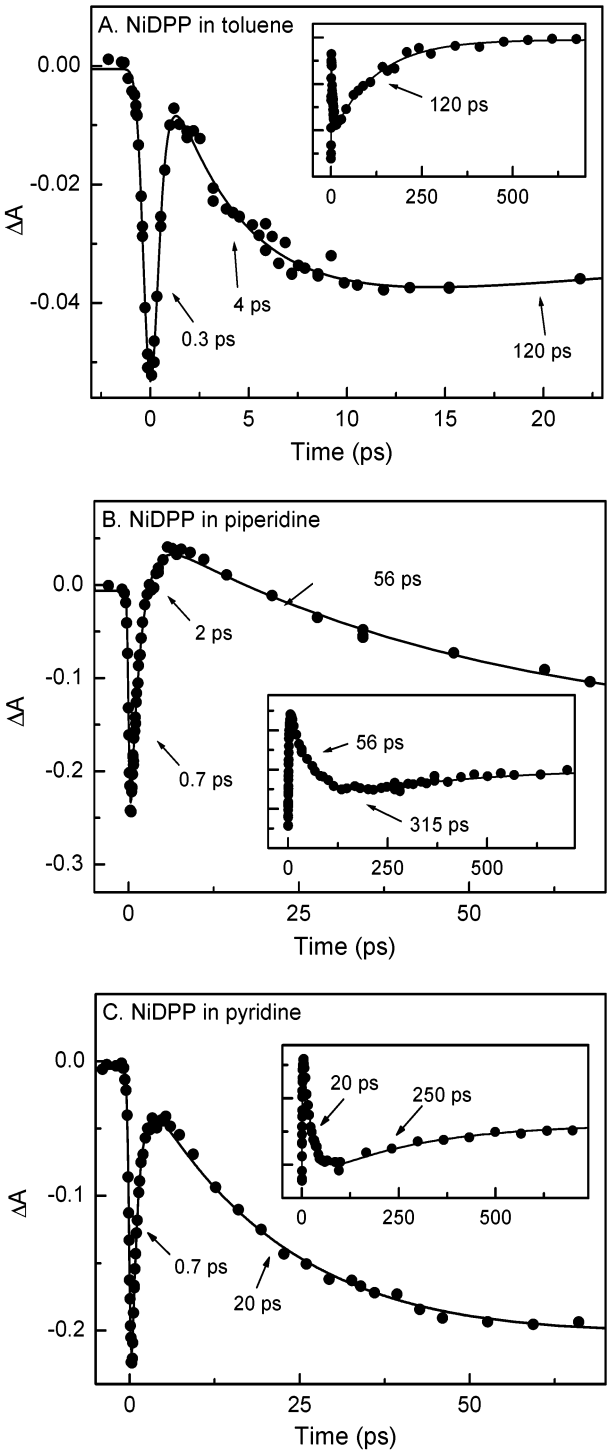

Figure 6. Representative kinetic data and fits to multiexponential functions plus the instrument response for NiDPP in toluene (A), piperidine (B), and pyridine (C) obtained at room temperature using 130-fs excitation flashes at 550 nm. For each solvent, the average values for the kinetic components from measurements probing at a variety of wavelengths are given in the text.

in the metal excited state over the next several picoseconds (processes *a* and *b* in Figure 1).

We assign the ~65 ps component as the *average* lifetime of the Ni*$(d_{z^2},d_{x^2-y^2})$ state in piperidine. As this state decays, its blue-shifted derivative-like spectrum transforms into a red-shifted derivative-like spectrum, with a new transient absorption band 20−25 nm to the red of the ground-state Soret position

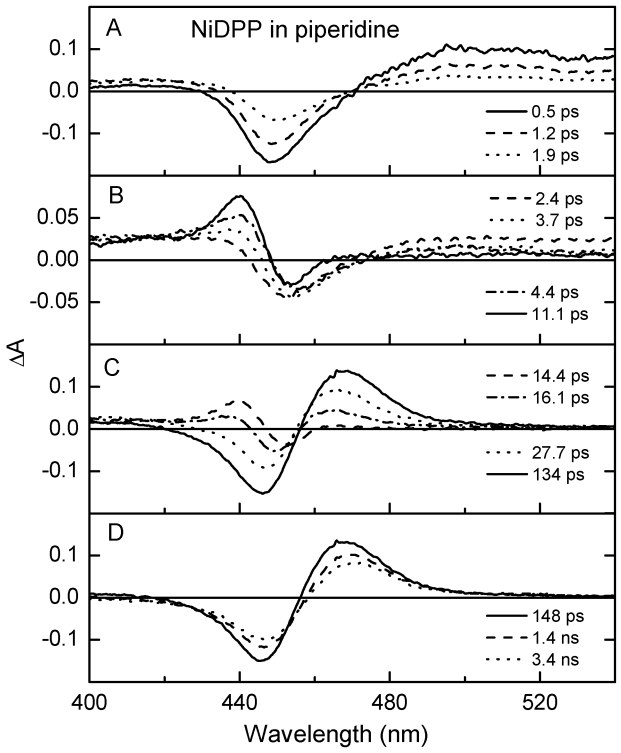

Figure 7. Soret-region transient absorption difference spectra for NiDPP in piperidine showing more details of the time evolution of the absorbance changes than are depicted in Figure 5B.

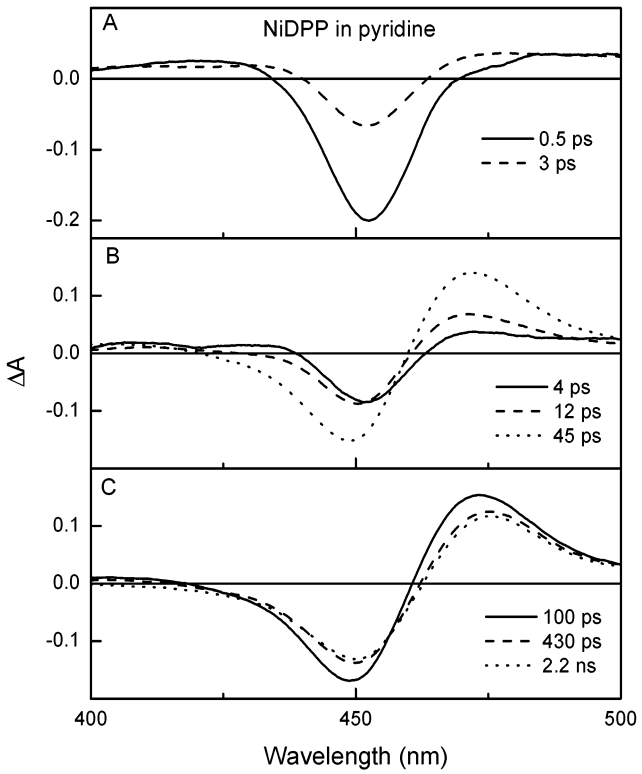

Figure 8. Soret-region transient absorption difference spectra for NiDPP in pyridine.

(Figures 5B and 7C). The position of this new absorption is the same as that observed when ligands are coordinated to (other) nickel porphyrins in the ground electronic state to form a six-coordinate, bis-ligated adduct (e.g., compare the ground-state spectra for $NiF_{20}DPP$ in piperidine and methylcyclohexane in Figures 4C and 4D, dashed lines).[14] Thus, the spectral changes that occur between ∼10 and ∼150 ps include the binding of piperidine ligand(s) to the metal by the four-coordinate Ni*-(d_{z^2},$d_{x^2-y^2}$) excited state to produce an intermediate I_1 (process *d* in Figure 1). The yield and the nature of I_1 (i.e., the electronic configuration and whether it is a five- or six-coordinate complex) will be discussed below. However, there is no doubt that such a transient intermediate is formed because there is a clear subsequent kinetic phase with an average time constant of roughly 200 ps that reflects at least in part the lifetime of I_1. During this kinetic phase, the derivative-shaped spectrum of the 5/6-coordinate complex undergoes a shift to slightly longer wavelengths, and an ∼25% decrease in both the transient-absorption and bleaching intensities (compare spectra at 148 ps and 1.4 ns in Figure 7D). We take this result to indicate an ∼25% recovery of the four-coordinate ground state via ligand ejection (processes *f* and *l* in Figure 1) in competition with formation of the final electronic/conformational ground state of the six-coordinate product (process *e*). Subsequent decay of the spectrum to the baseline and return of NiDPP to its original four-coordinate ground state takes >5 ns (process *n* in Figure 1).

(c) NiDPP in Pyridine. The time-resolved absorption changes for NiDPP in pyridine are shown in Figure 8 (Soret region) and Figure 9 (Q-band region). Representative kinetic data at 462 nm and a fit to three exponentials plus a constant (long-time asymptote) are shown in Figure 6C. The average time constants from single wavelength and global fits to the data between ∼450 and ∼480 nm to three or four exponentials are ∼0.7, ∼2, ∼25, and ∼200 ps, and the last phase again actually

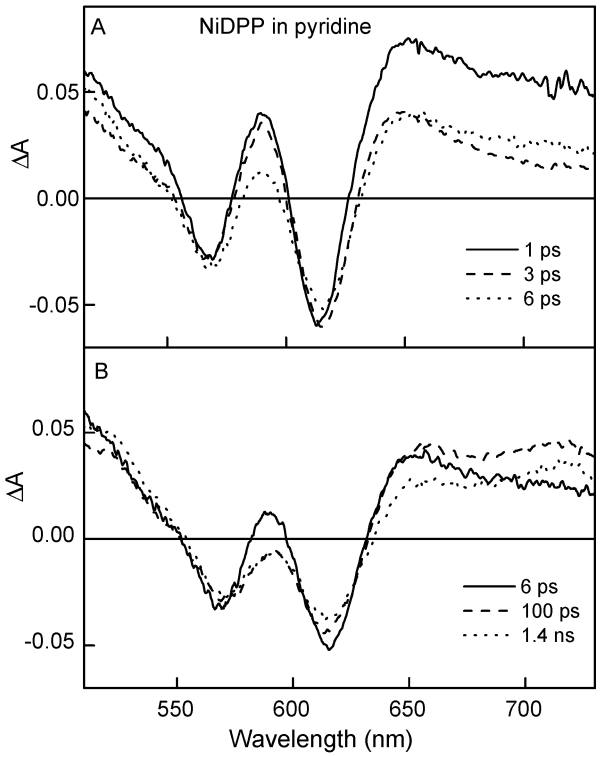

Figure 9. Representative transient absorption difference spectra in the Q-band region for NiDPP in pyridine obtained at room temperature using 200-fs excitation flashes at 425 nm.

takes on values in the range 100−400 ps as a function of probe wavelength. Overall the data are very similar to those for NiDPP in piperidine and indicate binding of pyridine ligands to the photoexcited four-coordinate nickel.

The spectrum observed immediately after excitation (Figure 8A, solid line) is very similar to those observed in toluene and piperidine at a similar time, and again can be assigned to formation of the macrocycle (P*) excited state upon photon absorption. The Soret bleaching decreases rapidly with an average time constant of ∼0.7 ps to give a spectrum of similar shape at 3−4 ps (Figure 8A, dashed line). This spectral evolution is somewhat different from that seen for NiDPP in piperidine and toluene, where at a few picoseconds the P* spectrum has already given way to the blue-shifted derivative-shaped spectrum of the Ni*(d_{z^2},$d_{x^2-y^2}$) metal excited state (see, e.g., Figure 7B). Such a spectrum is not observed in pyridine even though the formation of the Ni*(d_{z^2},$d_{x^2-y^2}$) state (as opposed to internal conversion to the ground state) must be the principal route for decay of the macrocycle P* state, as is observed in toluene and piperidine. In support of this idea, an average time constant of ∼0.7 ps is found for the spectral changes that occur in the Q-band region. When referenced to the broad transient absorption, it is seen that the Q-band bleachings do not appreciably decay over the first several picoseconds (Figure 9A). This observation indicates that little if any deactivation of P* to the ground state occurs. Hence, the substantial decrease in the amplitude of Soret band bleaching at ∼3 ps (Figure 7A) likely derives from formation of a Ni*(d_{z^2},$d_{x^2-y^2}$) state that has a Soret absorption that significantly overlaps (i.e., is little shifted from) the ground-state Soret bleaching, as has been found previously for NiOEP in pyridine.[36]

Formation of a derivative-shaped spectrum with a transient absorption band ∼25 nm to the red of the bleaching of the ground-state Soret band occurs with an average time constant of ∼25 ps (Figure 6C). By analogy to the situation for NiDPP in piperidine, this value is assigned as the nominal lifetime of the Ni*(d_{z^2},$d_{x^2-y^2}$) state, which includes ligand binding to form intermediate I_1 (process *d* in Figure 1). We note that the apparent lifetime of the metal excited state may be somewhat convolved with conformational/vibrational dynamics (process *b* in Figure 1) that require several picoseconds and can be resolved at some wavelengths as the second kinetic phase that has an ∼2 ps average, with values >10 ps at some wavelengths. The intermediate I_1, which again may be a five-coordinate species or an unrelaxed six-coordinate form, decays with an average time constant of roughly 200 ps and is accompanied by a slight red-shifting and ∼25% reduction in spectral amplitude (Figure 8C). These observations are similar to those found in piperidine, and again we suggest the decrease in spectral amplitude may reflect a competition between ligand loss by I_1 (process *f*) and formation of the electronic/conformational ground state of the six-coordinate product (process *e*). As I_1 decays, there is only a modest change in the magnitude of Q-band bleaching (Figure 9B). This finding indicates that, at least for NiDPP in pyridine, ligand loss (process *f*) is a relatively minor (≤25%) pathway compared to binding of a sixth ligand (if I_1 is five-coordinate)

(36) Such observations and conclusions concerning opposing Soret-region absorption changes and the effects on the amplitudes of features in the difference spectra are not uncommon for nickel porphyrins. Such effects no doubt contribute to the early-time spectral changes for NiDPP in toluene (Figure 5A) and have been discussed previously for NiT(t-Bu)P in noncoordinating solvents.[4b]

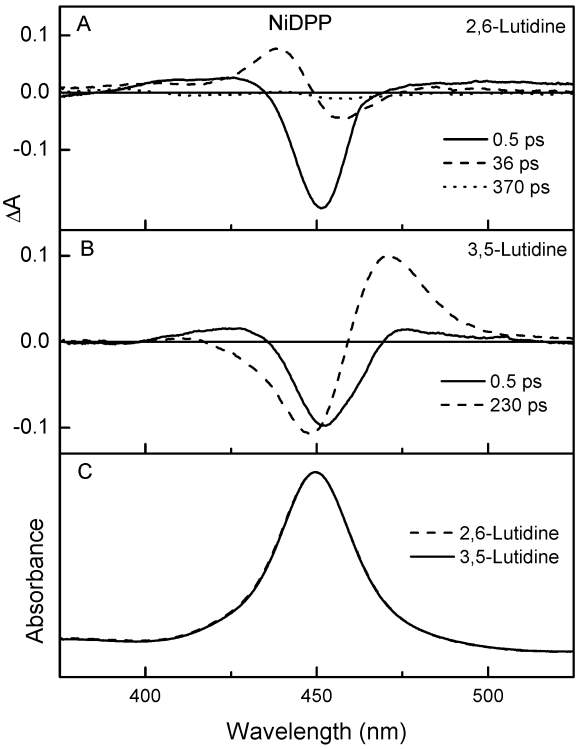

Figure 10. Soret-region transient absorption difference spectra at selected delay times for NiDPP in 2,6-lutidine (A) and 3,5-lutidine (B) at room temperature using 130-fs excitation flashes at 550 nm. Soret-region ground-state spectra of NiDPP in these solvents are shown in panel C.

or compared to vibrational/conformational relaxation of a six-coordinate I_1. The time course for re-formation of the original ground state of the four-coordinate NiDPP (process *n*) from the six-coordinate photoproduct was measured on a conventional flash-photolysis setup using 5-ns excitation flashes at 532 nm. The decay of both the transient absorption at 475 nm and the ground-state bleaching at 450 nm yielded an ∼25 ns time constant.

(d) NiDPP in 2,6-Lutidine and 3,5-Lutidine. The differences described above for the photoligation dynamics of NiDPP in piperidine and pyridine prompted us to investigate two pyridine derivatives, 2,6-lutidine and 3,5-lutidine, that should provide different degrees of steric hindrance toward ligand binding. As is the case for pyridine, it is clear that neither lutidine molecule coordinates to NiDPP in the ground state, since the position of the Soret band is the same as found in toluene (Figures 10C and 4A). The photophysics of NiDPP in 2,6-lutidine are essentially the same as that found in toluene as can be readily seen by comparison of the spectra in Figures 10A and 5A. The spectral and kinetic data thus indicate a convolution of P*Ni-(d_{z^2})^2 → PNi*(d_{z^2},$d_{x^2-y^2}$) internal conversion in <1 ps and relaxation requiring 10 ps or so within the metal excited state (processes *a* and *b* in Figure 1). The dotted spectrum in Figure 10A shows that by 370 ps the unligated PNi*(d_{z^2},$d_{x^2-y^2}$) metal excited state has returned to the ground state (process *c*). The lifetime of this state of ∼130 ps is essentially the same as the value of ∼120 ps found in toluene. The results thus show that 2,6-lutidine does not coordinate to NiDPP in either the ground or excited electronic states, and we suggest that the presence of the two methyl groups on the carbons adjacent to the nitrogen hinders coordination to the nickel(II) ion in the macrocycle.

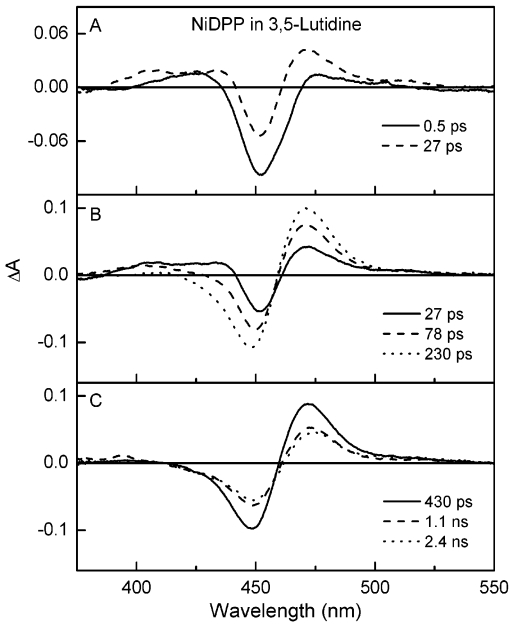

Figure 11. Soret-region transient absorption difference spectra for NiDPP in 3,5-lutidine showing more details of the time evolution of the absorbance changes than are depicted in Figure 10B.

In contrast, the excited-state dynamics of NiDPP in the less sterically hindered 3,5-lutidine are similar to those found in pyridine, as can be seen by comparing the spectra in Figures 10B and 11 with those in Figure 8. The lowest $^1(\pi,\pi^*)$ excited state (P*) of the macrocycle (Figures 10B and 11A, solid lines) decays largely by $P^*Ni(d_{z^2})^2 \rightarrow PNi^*(d_{z^2},d_{x^2-y^2})$ internal conversion ($\leq$0.7 ps) followed by vibrational/conformational relaxation (2−10 ps) (processes *a* and *b* in Figure 1). The $PNi^*(d_{z^2},d_{x^2-y^2})$ metal excited state then decays with a nominal lifetime of ∼85 ps in part by ligand acquisition (process *d*) leading to the formation of a derivative-shaped spectrum featuring an excited-state absorption ∼20 nm to the red of the ground-state bleaching (230 and 430 ps spectra in Figure 11). This spectrum at ∼450 ps reflects the five- or six-coordinate intermediate I_1, which has a nominal lifetime of ∼550 ps in 3,5-lutidine. As I_1 decays, its derivative-shaped spectrum undergoes a small red shift and an ∼50% decrease in amplitude (Figure 11C) that we assign to a competition between ligand ejection by five- or six-coordinate I_1 to re-form the four-coordinate unligated species (process *f*) and formation of the electronically/conformationally relaxed ground state of six-coordinate adduct (process *e*). Ligand release by the six-coordinate photoproduct to re-form the original unligated species (process *n*) again occurs on a time scale of many nanoseconds.

(e) $NiF_{20}DPP$ in Toluene, Pyridine, and Piperidine. Photoexcited $NiF_{20}DPP$ and $NiF_{28}DPP$ in toluene decay via the same combination of processes *a*, *b*, and *c* (Figure 1) as reported above for NiDPP in toluene, with respective similar probe-wavelength-dependent time constants with average values of <0.7 ps, ∼4 ps, and ∼120 ps time constants (data not shown). The transient spectra are also essentially the same as those for NiDPP in toluene (Figure 5A) but blue-shifted in keeping with the blue-shifted position of the ground-state Soret band (compare Figures 4A and C, solid lines).

Figures 12A and 12B show Soret-region transient absorption spectra for $NiF_{20}DPP$ in piperidine and pyridine, respectively. As described above, ∼80% of the $NiF_{20}DPP$ molecules in piperidine are six-coordinate $NiF_{20}DPP(pip)_2$ and the remainder is unligated. In pyridine, ∼65% are in the $NiF_{20}DPP(pyr)_2$ form. Both are evidenced by the ∼20 nm red shifts in the ground-state Soret absorption in these solvents relative to toluene (Figures 4C and 4D). The transient difference spectra obtained immediately after excitation show ground-state bleaching of the six-coordinate species (Figures 12A and 12B, solid lines) due to formation of the $P^*Ni^T(d_{z^2},d_{x^2-y^2})L_2$ macrocycle excited $^1(\pi,\pi^*)$ state (Figure 1, right). A small decrease in the Soret bleaching is accompanied by the formation of a transient absorption band ∼20 nm to shorter wavelengths with an average time constant of ∼2 ps, followed by minor spectral changes with an average time constant of ∼30 ps to give the spectra shown at 100 ps in Figures 12A and 12B (dashed lines). The new transient absorption to the blue of the Soret bleaching is similar in position to the ground-state Soret band of nonligated $NiF_{20}DPP$ in toluene (Figure 4C). This finding indicates that the photoexcited $NiF_{20}DPP(L)_2$ complexes have dissociated to give four-coordinate $NiF_{20}DPP$ plus the free nitrogenous-base ligands. As described above, the overall photodissociation likely involves the formation, relaxation, and decay of several electronic intermediates (via processes *g*, *h*, *i*, and *k* in Figure 1) including intermediate I_2 that is either a five-coordinate or unrelaxed four-coordinate form ultimately leading to the final four-coordinate product (process *l*). Given the rapid production of the Soret absorption of the deligated species from the initially excited $P^*Ni^T(d_{z^2},d_{x^2-y^2})L_2$ state without clear spectral detection of the ligated intermediates shown in Figure 1 (right), it is apparent that the early electronic events including the loss of the ligands occur in several picoseconds or less and that vibrational/conformational processes span several to tens of picoseconds. Spectra taken at ∼3.5 ns (not shown), which is the limit of the apparatus, are virtually unchanged from the ones observed at 100 ps in Figures 12A and 12B. These results indicate that the return of $NiF_{20}DPP$ to its original ligated six-coordinate electronic ground state (which requires ligand binding as well as nuclear and electronic relaxations) takes greater than 5 ns (process *m* in Figure 1). Results similar to these were obtained for $NiF_{28}DPP$ in pyridine.

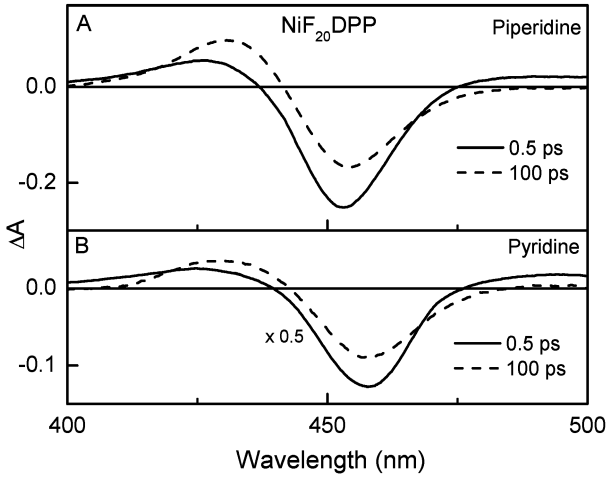

Figure 12. Soret-region transient absorption difference spectra at selected delay times for $NiF_{20}DPP$ in piperidine (A) and pyridine (B) at room temperature using 130-fs excitation flashes at 550 nm.

Discussion

The porphyrin macrocycle can be deformed into a variety of nonplanar structures (saddle, ruffle, dome, wave, and combinations) via steric interactions involving multiple and/or bulky peripheral substituents.[25−27,37] Even the simplest nonplanar porphyrins—closed-shell metal complexes such as zinc(II) chelates, free-base forms bearing two central protons, or diacid derivatives containing four central protons—exhibit significant differences in photophysical properties compared to their nominally planar counterparts.[20−24] These differences include dramatically shortened excited-state lifetimes and diminished fluorescence yields (derived from enhanced nonradiative deactivation of the lowest $^1(\pi,\pi^*)$ excited state) as well as red-shifted and broadened optical absorption and emission bands with unusually large absorption-fluorescence spacings (Stokes shifts). Additionally, there is a much stronger dependence of all these properties on solvent polarity, viscosity, and temperature than observed for planar porphyrins. In the most general terms, these differences can be ascribed to the ability of nonplanar porphyrins to adopt multiple conformations in both the ground and excited states overlaid with a propensity for photoinduced conformational changes. Studies to date have made it clear that the complexity and diversity of the photophysical behavior observed for nonplanar porphyrins derives from the extremely strong interplay of both structural and electronic factors contributed by the macrocycle, peripheral substituents, and solvent (even nonpolar solvents).[4b,23b,24] The cause and effect relationships among these parameters are very entangled. This recognition represents an overriding consideration in understanding the photophysical behavior of nonplanar porphyrins. In the present paper, we have taken a first step in probing how these relationships impact the photoinduced metal−ligand binding and release phenomena of nonplanar nickel porphyrins.

(a) Binding of Ligands by Photoexcited NiDPP. We have shown here that although nonplanar NiDPP does not bind ligands in the ground electronic state, photoexcitation induces ligation and that the binding events depend on the characteristics of the ligand (steric constraints, flexibility, basicity, aromaticity, planarity, etc). To focus on these issues, we will not re-visit the internal conversion and conformational/vibrational relaxation dynamics that take place on the ≤20 ps time scale (processes *a* and *b*). Nor will we analyze the ultimate re-formation of the unligated ground state on the multi-nanosecond time scale (process *n*). Rather we will focus on new insights gained from these studies, which include (1) the resolution of the unligated metal PNi*(d_{z^2},$d_{x^2-y^2}$) excited state prior to ligand binding and (2) the finding of a ligated intermediate whose formation and decay characteristics depend on ligand properties.

Although formation of the PNi*(d_{z^2},$d_{x^2-y^2}$) metal excited state from the P*Ni(d_{z^2})^2 macrocycle excited state is well documented for nickel porphyrins in non-coordinating solvents, previously there has been scant evidence for formation of this intermediate prior to ligand acquisition, such as for NiOEP in pyridine. The reasons may involve spectral and/or kinetic congestion, including the relative time scales of internal conversion, conformational/vibrational relaxation, and ligand binding. In this regard, one of the highlights of our studies here is the clear spectral/kinetic resolution for NiDPP in piperidine of the four-coordinate (nonligated) PNi*(d_{z^2},$d_{x^2-y^2}$) excited state. We find a dramatic time evolution of the absorption difference spectra (Figure 5B) diagnostic of processes *a* and *d* in Figure 1 that connect the three states P*Ni(d_{z^2})^2 → PNi*(d_{z^2},$d_{x^2-y^2}$) → intermediate I_1, where I_1 is a five-or six-coordinate transient as discussed below. The ability afforded by nonplanar NiDPP to resolve the four-coordinate Ni*(d_{z^2},$d_{x^2-y^2}$) metal excited state in a strongly coordinating medium opens opportunities for study of the rates, yields, and mechanisms of photoassociation and how these factors depend on the inter-related structural/electronic properties of the porphyrin and ligand.

A second manner in which the results presented here extend previous work on ligand association to photoexcited planar porphyrins is the finding of clear kinetic evidence for intermediate I_1. The two simplest assignments for this intermediate are as follows. (1) I_1 is a five-coordinate species, with decay processes *f* and *e* representing the competition between ligand loss and binding of the sixth ligand (second axial ligand), respectively. (2) I_1 is six coordinate, with process *f* again representing ligand loss (in this case of both ligands) and process *e* representing vibrational/conformational relaxation to give the bis-ligated ground-state photoproduct. These two assignments are probably overly simplified and the true situation is that I_1 may actually involve more than one state/conformer since (A) the binding of the first and second ligands may not be temporally well delineated from each other or from conformational/vibrational relaxations and (B) multiple conformers involving various degrees of ruffle/saddle/etc distortions likely contribute, as suggested by work on nonplanar porphyrins, including NiDPP in nonligating solvents (see Introduction). In addition, photoproduct formation (processes *d* plus *e*) must involve a spin flip to convert the Ni*(d_{z^2},$d_{x^2-y^2}$) metal *singlet* excited state to the *triplet* ground-state Ni^T(d_{z^2},$d_{x^2-y^2}$)L_2 of the six-coordinate adduct. The contribution of these species/events probably underlies the rich and complex spectral/kinetic behavior that we observe. Despite these issues, the data readily support two key conclusions concerning intermediate I_1: (i) there is likely a significant contribution from the elusive five-coordinate form and (ii) trends in the formation time and in the decay time/pathways correlate with the properties of the ligand.

In the simplest model, intermediate I_1 forms from the PNi*(d_{z^2},$d_{x^2-y^2}$) metal excited state, which has a lifetime given by this ligand-binding event (process *d* in Figure 1) in competition with internal conversion to the ground state (process *c*). The lifetime of PNi*(d_{z^2},$d_{x^2-y^2}$) clearly depends on the ligand, with rough average lifetimes for NiDPP in pyridine, piperidine, and 3,5-lutidine of ∼25, ∼65, and ∼80 ps, respectively (Table 1, column 4). Using these values and assuming that process *c* has the rate constant (120−130 ps)$^{-1}$ found in toluene and 2,6-lutidine gives a rate constant and yield for the formation of I_1 via ligand binding process *d* of ∼(30 ps)$^{-1}$ and ∼80% in pyridine, ∼(140 ps)$^{-1}$ and ∼ 50% in piperidine, and ∼(300 ps)$^{-1}$

(37) References to additional representative Zn and free base nonplanar porphyrins. (a) Medforth, C. J.; Senge, M. O.; Smith, K. M.; Sparks, L. D.; Shelnutt, J. A. *J. Am. Chem. Soc.* **1992**, *114*, 9859. (b) Nurco, D. J.; Medforth, C. J.; Forsyth, T. P.; Olmstead, M. M.; Smith, K. M. *J. Am. Chem. Soc.* **1996**, *118*, 10918. (c) Barkigia, K. M.; Nurco, D. J.; Renner, M. W.; Melamed, D.; Smith, K. M.; Fajer, J. *J. Phys. Chem. B* **1998**, *102*, 322. (d) Senge, M. O. *Z. Naturforsch* **1999**, *54b*, 821. (d) Regev, A.; Galili, T.; Medforth, C. J.; Smith, K. M.; Barkigia, K. M.; Fajer, J.; Levanon, H. *J. Phys. Chem.* **1994**, *98*, 2520. (e) Barkigia, K. M.; Berber, M. D.; Fajer, J.; Medforth, C. J.; Renner, M.; Smith, K. M. *J. Am. Chem. Soc.* **1990**, *112*, 8851. (f) Ema, T.; Senge, M. O.; Nelson, N. Y.; Ogoshi, H.; Smith, K. M. *Angew. Chem. Int. Ed. Engl.* **1994**, *33*, 1879. (g) Senge, M. O.; Ema, T.; Smith, K. M. *J. Chem. Soc., Chem. Commun.* **1995**, 733.

Table 1. Summary of Photophysical Data for NiDPP[a]

solvent[b]	P* lifetime (process *a*) (ps) [c]	Ni*(d_{z^2},$d_{x^2-y^2}$) relaxation (process *b*) (ps)[d]	Ni*(d_{z^2},$d_{x^2-y^2}$) lifetime (processes *c* and *d*) (ps)[e]	intermediate I_1 lifetime (processes *e* and *f*) (ps)[f]	intermediate I_1 fractional decay to the 6-coordinate ground-state (process *e*)[g]	intermediate I_1 fractional decay to the 4-coordinate ground-state (process *f*)[h]	ligand release from the 6-coordinate ground state (process *n*) (ns)[i]
pyridine	<1	~2	25 (15−35)	200 (70−350)	0.75	0.25	~25
piperidine	<1	~3	65 (40−90)	200 (70−350)	0.75	0.25	>5
3,5-lutidine	<1	~4	80 (70−90)	550 (500−600)	0.55	0.45	>5
2,6-lutidine	<1	~5	130 (120−140)	NA	NA	NA	NA
toluene	<1	~4	120 (100−140)	NA	NA	NA	NA

[a] All data are at room temperature. The processes indicated in the column headings refer to those shown in Figure 1. As described in the text and the notes below, multiple processes and conformers likely contribute on each time scale and on overlapping time scales, and contribute to the complex spectral and kinetic data. These contributions are reflected in part in the ranges of probe-wavelength-dependent values (in parentheses), for which rough weighted average values are also listed as a guide to more readily show trends for the ligands. NA = not applicable (see footnote b). [b] Toluene and 2,6-lutidine do not axially coordinate to NiDPP in either the ground or excited state. Pyridine, piperidine, and 3,5-lutidine also do not coordinate to in the ground state, but do so following photoexcitation. [c] Probe-wavelength-dependent values in the range 0.3−1.5 ps are observed for the first time constant resulting from multiexponential fitting of the kinetic data, with the range depending on solvent. Each value listed is a rough weighted average and is taken to be as an upper limit on the lifetime of the $^1(\pi,\pi^*)$ macrocycle P*Ni(d_{z^2})^2 excited state due to convolution with the subsequent vibrational/conformational relaxation in the metal PNi*(d_{z^2},$d_{x^2-y^2}$) excited state. [d] Probe-wavelength-dependent values ranging from ~1 to >10 ps are observed for the second time constant, with the range depending on solvent. The values listed are rough weighted average values. [e] Lifetime of the PNi*(d_{z^2},$d_{x^2-y^2}$) metal excited state. [f] Lifetime of intermediate I_1. [g] The fraction of intermediate I_1 that decays to the six-coordinate ground-state photoproduct. [h] The fraction of the intermediate I_1 that decays by re-formation of the original four-coordinate ground-state starting material. [i] Lifetime of the six-coordinate photoproduct with regard to loss of the two acquired ligands to regenerate the original four-coordinate ground state. Lifetimes >5 ns are deduced for each coordinating solvent from the transient absorption data (which extends to ~3.5 ns). The value for NiDPP in pyridine was obtained from nanosecond flash photolysis measurements.

and ~35% in 3,5-lutidine. Experimentally, it is difficult to unambiguously assay the yield of I_1 due to spectral and kinetic congestion, but our best estimates using matched conditions give the same trend in yield but with less difference than calculated above (i.e., 80%, 70%, 60%). This difference is not surprising, considering that the PNi*(d_{z^2},$d_{x^2-y^2}$) lifetimes encompass probe-wavelength-dependent ranges of values (Table 1), likely reflecting the physical origins mentioned above (multiple contributing conformers, temporal overlap of binding of the first and second ligand and relaxation processes, etc.). Hence, these simple calculations are consistent with the trends seen directly from the observed time scales for decay of the precursor metal excited state and indicate that photoinduced ligand binding to NiDPP depends on interactions of the macrocycle/substituents with the ligand via its steric hindrance, aromaticity, etc.

Trends with ligand characteristics are also seen in the decay time scale of intermediate I_1, which has rough average lifetimes of ~200, ~200, and ~550 ps in pyridine, piperidine, and 3,5 lutidine, respectively (Table 1, column 5). The lifetime of intermediate I_1 is given by the rate constants of two decay pathways, namely, formation of the ground state of the final bis-ligated six-coordinate photoproduct by binding a second ligand and/or relaxation of the six-coordinate species (process *e* in Figure 1) in competition with re-formation of the original unligated, four-coordinate species (process *f*). Columns 6 and 7 of Table 1 list the relative yields of these pathways (obtained above from the reduction in the spectral amplitudes as I_1 decays).[38] On the basis of the I_1 average lifetimes and fractional decay yields, it is seen that the dissociation route (process *f*) has an average rate constant of about $(1\ \text{ns})^{-1}$ independent of ligand, whereas the average rate constant of the photoproduct route (process *e*) is about 3-fold smaller with the sterically hindered ligand 3,5-lutidine compared to pyridine or piperidine [$\sim(300\ \text{ps})^1$ versus $\sim(1\ \text{ns})^{-1}$]. It is not surprising that the loss of the ligand(s) at an intermediate stage may be a barrierless process and thus not be particularly sensitive to steric encumbrance on the ligand. On the other hand, the photoproduct pathway may very well involve the traversing of one or more barriers (involving conformational readjustments of the porphyrin and ligands) whose heights are greater when steric constraints are present. Thus, even considering the complexities noted above, the trends in the estimated average rate constants are in keeping with the trends in the observed lifetimes in demonstrating that the decay of intermediate I_1, like the time scale for its formation, depends strongly on ligand properties.

The results also suggest that a five-coordinate species makes a strong contribution to intermediate I_1 (perhaps in addition to a conformationally/vibrationally unrelaxed six-coordinated form). These findings include the observed spectra shifts that accompany the I_1 decay as well as the finding that the I_1 lifetime is longer (and the apparent rate constant for the photoproduct channel smaller) for the sterically encumbered 3,5-lutidine compared to its simple pyridine analogue. Evidence for five-coordinate adducts of planar nickel porphyrins is rare, although these species are thought to form in certain circumstances.[3b,13,15] No five-coordinate transient, or any transient intermediate at all, has previously been reported for ligand binding to photoexcited planar nickel porphyrins such as NiOEP in pyridine.[7a,9b,c] Some workers have suggested that a five-coordinate intermediate may be present but that it loses the ligand before a second one is coordinated, i.e., binding of the second ligand is overall rate

(38) The magnitudes of the absorbance changes also may be modulated during the final stages of the ligation process as a consequence of the structural, vibrational, and electronic relaxations within the six-coordinate photoproduct and readjustments in the surrounding solvent molecules and their interactions with the porphyrin. Such spectral changes may lead to diminished amplitudes of certain features in the spectrum (due to decreased extinction coefficients or increased overlap of opposing absorptions and bleachings) and complement diminished amplitudes derived from return of molecules to the original four-coordinated ground state via ligand loss.

limiting for the planar NiOEP.[9b] Our results on NiDPP clearly indicates that the yield of the final six-coordinate adduct from I_1 is high, $\geq$50%. Work with other ligands and strapped or capped nonplanar nickel porphyrins having differing degrees of steric hindrance, conformational flexibility, and ligand accessibility will further examine this issue.

(b) General Structural-Electronic Considerations. Several structural considerations are generally relevant to this work (see Introduction[33]). One is that unligated, low-spin NiDPP and $NiF_{20}DPP$ (and probably $NiF_{28}DPP$) are especially flexible and thus may adopt more than one conformation in the ground and excited states in solution. Another is that population of the metal excited state with $d_{x^2-y^2}$ occupancy must result in a significant expansion of the equatorial Ni−N distances with some readjustment of the macrocycle distortion(s). Conversely, relaxation from the metal excited state or photodeligation will cause a contraction of the long porphyrin Ni−N distances, which will allow the macrocycle to relax via several, possibly more distorted, conformations. These and other effects can readily lead to spectral heterogeneity and the probe-wavelength-dependent kinetics of the excited-state dynamics that we have reported here.

Photoinduced ligation and deligation will be especially susceptible to steric crowding of the 12 phenyl rings around the periphery of the macrocycle and can be expected to (1) affect the approach and access of a potential ligand to the metal site, (2) exacerbate the effects of steric encumbrance and flexibility of the ligand itself, and (3) influence the ability of the porphyrin to conformationally and electronically adjust to accommodate coordination. As can be seen from the structural data in Figure 2, the peripheral phenyl rings of NiDPP encumber the macrocycle's face. Previous studies of NiDPP, ZnDPP, and H_2DPP indicate that these peripheral rings have $\pi-\pi$ interactions with one another[24,39] that probably adjust to some degree for axial ligation to occur. These steric/electronic effects probably contribute substantially to the first stages of ligand binding being faster in pyridine ($\sim$25 ps) than in 3,5-lutidine ($\sim$80 ps).

Our results indicate that there are also electronic interactions between the peripheral phenyl rings (and/or macrocycle) of NiDPP and potential metal axial ligands that depend on ligand (solvent) characteristics. We have found that the initial stage of ligand binding generally occurs faster in pyridine ($\sim$25 ps) than in piperidine ($\sim$65 ps) even though the latter molecule is a much stronger base. This result suggests that the aromatic pyridine ligands may have interactions with the aromatic peripheral phenyl rings and/or the macrocycle that favorably disposes them toward subsequent binding of NiDPP to the nickel, whereas the nonaromatic solvent piperidine does not. Such an interaction includes (but is not limited to) potential π-stacking between the solvent and the phenyl groups on the porphyrin. As a result, the pyridine molecules may be "standing by" and perhaps cause the overall porphyrin structure to be somewhat preadjusted so that pyridine molecules can rapidly bind to the metal center following photoexcitation.

Support for porphyrin−solvent interactions can been seen in the ground-state absorption spectra of NiDPP in aromatic versus nonaromatic solvents. In particular, the spectra in toluene and pyridine are similar to one another, but both are shifted from those in their nonaromatic counterparts methylcyclohexane and piperidine (Figures 4A and 4B). On the other hand, the ground-state spectra for the dodecasubstituted porphyrin NiOETPP are the same in toluene and methylcyclohexane (Figure 3A). These findings indicate that the interactions between the aromatic solvents and NiDPP must derive in part from the presence of its 8 β phenyl rings. Additional insights can be gleaned from the crystal structures of NiDPP.[25b,c] These data show that the adjacent β phenyl groups (on the same pyrrole ring) are spread apart such that each β phenyl group is actually closer to its nearest *meso* phenyl group (Figure 2). This splitting of the β phenyl groups may open spaces around the periphery of the porphyrin macrocycle that solvent molecules can at least partially fill. Such interactions would be most favorable for aromatic (and planar) solvents such as pyridine, which might be able to partially sandwich between two β aromatic phenyl groups. In contrast, nonaromatic, nonplanar, and more flexibile solvent molecules such as piperidine would have reduced interactions and perhaps also a poorer fit with the porphyrin cavity.

In addition, there may be an equilibrium population of solvent molecules (and particularly aromatic ones) in the "pockets" formed by the 12 phenyl rings. Potential ligands may be transiently held by multiple π-interactions with the peripheral groups and the macrocycle without actually being bound to the metal. Supporting evidence for such a possibility derives from crystallographic data for the (py)Cu(II)OETPP$^{+\bullet}$py π-cation radical, which shows both a "proximal" pyridine axial ligand bound to the metal as well as a pyridine "solvate" tucked into the "distal" pocket but with the pyridine-nitrogen pointing away from the Cu, and thus clearly intercalated into the porphyrin superstructure but not coordinated to the metal.[40] Such preorganization may be favored for aromatic solvents and would facilitate ligand binding after photoexcitation compared to ligands that cannot have the same types of interactions with the porphyrin. Work is now underway to understand the steric/electronic role played by the β phenyl rings of NiDPP toward ligand binding by carrying out studies on NiOETPP and other dodecasubstituted porphyrins in potentially coordinating solvents. These studies will also probe the extent to which the ability to access various structural distortions inferred from the X-ray data for the dodecasubstituted nickel porphyrins affects the ligand-photoassociation dynamics.

A final point worth noting is that although it is thought that ligand binding to photoexcited four-coordinate *planar* nickel porphyrins requires changes in conformation and electron density that occur in the Ni*(d_{z^2},$d_{x^2-y^2}$) excited state,[4,8,9b] it is very possible that ligand attachment to *nonplanar* nickel porphyrins begins in part in the macrocycle $^1(\pi,\pi^*)$ excited-state P*Ni(d_{z^2})^2 initially produced upon photon absorption. As described in the Introduction, it has been well documented that nonplanar zinc and free base porphyrins undergo photoinduced conformational changes and access multiple configurations (involving the macrocycle, peripheral groups and solvent) in the macrocycle's $^1(\pi,\pi^*)$ excited state.[22−24] We have measured these excursions to take several picoseconds or longer for H_2-DPP and several fluorinated analogues.[24] As a result of this conformational flexibility, photoexcitation of NiDPP may

(39) Variable-temperature NMR results indicate that interactions between the peripheral aryl groups in DPP versus $F_{20}DPP/F_{28}DPP$ can modify the barriers for β-aryl rotation and macrocycle inversion. Medforth, C. J.; Nurco, D. J.; Smith, K. M. Unpublished results.

(40) Renner, M. W.; Barkigia, K. M.; Fajer, J. *Inorg. Chim. Acta* **1997**, *263*, 181.

produce directly a macrocycle excited-state geometry and electron density that is favorable for ligand binding while the ground-state does not allow coordination. Hence, ligand binding may occur both from the macrocycle and metal excited states of nonplanar nickel porphyrins, although only the binding to the metal state is explicitly shown in Figure 1 (process *d*) and appears to be the essentially exclusive route for planar analogues.

In summary, the studies presented here have probed how the structural and electronic effects induced by the peripheral substituents in NiDPP, NiF_{20}DPP, and NiF_{28}DPP as well as the characteristics of potential axial ligands (sterics, basicity, aromaticity, planarity) modulate metal coordination in the ground electronic state, coordination of axial ligands following photon absorption by unligated porphyrins (NiDPP), and photoejection of ligands coordinated in the ground state (NiF_{20}DPP and NiF_{28}DPP). In addition to the new insights gained, this study highlights new opportunities for exploring these issues by making use of the intimate relationships that exist between structural/electronic factors associated with the macrocycle/substituents/solvent in controlling the photodynamics of nonplanar porphyrins. These relationships and the concepts described above concerning porphyrin conformational flexibility and the corresponding structural/electronic characteristics of the medium may well be generally applicable to distorted open-shell metallo-tetrapyrroles and therefore relevant to a variety of biologically and biomimetically important processes involving these complexes.

Acknowledgment. This work was supported by grants from the National Institutes of Health (GM34685 to D.H.), National Science Foundation (CHE-99-04076 to K.M.S., CHE-024336 to C.M.D.), and Civilian Research and Development Fund (BC1-105 to V.S.C. and D.H.) and the Division of Chemical Sciences, Geosciences and Biosciences, Office of Basic Energy Sciences, U.S. Department of Energy, under contract DE-AC02-98CH10886 at Brookhaven. C.J.M. thanks Prof. J. A. Shelnutt (Sandia National Laboratories/University of Georgia) for financial support and for many stimulating discussions. This work was partially supported by the Division of Materials Sciences and Engineering, Office of Basic Energy Sciences, U.S. Department of Energy. Sandia is a multiprogram laboratory operated by Sandia Corporation, a Lockheed-Martin Company, for the U.S. Department of Energy under contract DE-ACO4-94AL85000. V.S.C. thanks the Belarusian Foundation of Basic Research (Grants F00-100 and F02R-105) and Belarus State Program of Basic Research (Project Spektr-07) for financial support.

JA020611M